Branched Fibrous Amidoxime Adsorbent with Ultrafast Adsorption Rate and High Amidoxime Utilization for Uranium Extraction from Seawater

Wanning REN[1], Xinxin FENG[2,3], Yulong HE[2,3], Minglei WANG[2,3], Wanfeng HONG[4], Hongwei HAN[5], Jiangtao HU[2*] & Guozhong WU[1,2*]

[1] School of Physical Science and Technology, ShanghaiTech University, No. 393, Huaxia Middle Road, Pudong New Area, Shanghai 200031, P. R. China

[2] Shanghai Institute of Applied Physics, Chinese Academy of Sciences, No. 2019, Jialuo Road, Jiading District, Shanghai 201800, P. R. China

[3] University of Chinese Academy of Sciences, Beijing 100049, P.R. China

[4] College of Science, University of Shanghai for Science and Technology, Shanghai 200093, P. R. China

[5] College of Science, Shanghai University, Shanghai 200444, P. R. China

Wanning REN: Methodology, Writing - original draft, Conceptualization, Formal analysis;
Xinxin FENG: Formal analysis;
Yulong HE: Investigation;
Minglei WANG: Software was used;
Wanfeng HONG: Data curation;
Hongwei HAN: Visualization;
Jiangtao HU: Methodology, Writing - review & editing, Formal analysis;
Guozhong WU: Conceptualization, Supervision.

Abstract

Objective: We herein fabricated a branched structure containing AO groups on polypropylene/polyethylene spun-laced nonwoven (PP/PE SNW) fibers using grafting polymerization induced by radiation (RIGP) to improve AO utilization.

Methods: The chemical structures, thermal properties, and surface morphologies of the raw and treated PP/PE SNW fibers were studied. The adsorption properties were investigated using batch adsorption experiments in simulated seawater with an initial uranium concentration of 500 $\mu g \cdot L^{-1}$ (pH 4, 25 °C).

Results: The maximum adsorption capacity of the adsorbent material was 137.3 $mg \cdot g^{-1}$ within 24 h; moreover, the uranyl removal reached 96% within 240 min.

Limitations: Only simulated seawater adsorption experiments have been conducted, and real seawater adsorption experiments are yet to be conducted.

Conclusions: The adsorbent had an AO utilization rate of 1/3.5 and was stable over a pH range of 4–10, with good selectivity and reusability, demonstrating its potential for seawater uranium extraction.

Keywords: Radiation graft technology; Branching structure; High amidoxime utilization; Seawater uranium extraction; Ultrafast adsorption

1. Introduction

Nuclear power can play a major role in transitioning the energy supply to carbon neutrality because it does not produce greenhouse gases. The fundamental resource used by the nuclear energy industry is uranium, and its acquisition is crucial for the sustainability of green technologies [1, 2]. The primary source of uranium is terrestrial uranium mines that are expected to be exhausted within 100 years, irrespective of the increase in consumption rates [3]. Therefore, unconventional uranium sources are urgently required to ensure a stable supply of nuclear fuel. Generally, uranium occurs naturally, deposited in terrestrial ores or dissolved in seawater [4, 5]. The ocean contains 4.5 billion metric tons of U and is the largest uranium reserve on Earth, approximately 1,000 times that of terrestrial ores [6-8]. Thus, recovering uranium from seawater is a viable strategy for alleviating uranium shortages and stabilizing market prices. Although many strategies have been used since 1950s to recover uranium from seawater, extraction using sorbents is the most feasible method [9-11]. However, effective and selective uranium collection by adsorption is affected by extremely low uranium concentrations (~3.3 ppb) [12], severe interference from high levels of coexisting ions [13], high salinity, and microorganism contamination, ocean currents, and the complex, changeable marine environment [14]. The low use efficiency of the adsorption functional groups on an adsorbent (approximately 1% for fibrous adsorbents) is also a critical factor influencing the performance of adsorption materials [3, 15]. Among the various 200 uranium adsorption organic functional groups, the amidoxime (AO) group was selected as the most suitable ligand for uranium enrichment because of its high adsorption capacity [16, 17], excellent selectivity [18, 19], and relatively low cost. Various AO-based polymeric uranium adsorbents are fabricated, including membranes, resins, and fibers. Fibrous adsorbents remain at the forefront of adsorbent materials because of their high mechanical strength, high specific surface area, and ease of deployment and recycling [20].

Radiation graft polymerization is widely used in the preparation of fiber adsorbents because of its fast processing speed [21], uniform formation of active sites that initiate grafting, ability to endow materials with new performance characteristics, and, most importantly, suitability for large-scale industrial applications [22]. In pursuit of high adsorption capacity, researchers have focused on improving the degree of grafting (DG) of fibers. Saito et al. developed a fiber adsorbent with an acrylonitrile (AN) grafting ratio >595%; however, its maximum uranium adsorption capacity was only 3.02 $mg \cdot g^{-1}$ [23, 24]. The results [25-27] from classical AO-based adsorbent studies demonstrate that the adsorption capacity does not increase with an increase in DG. AO-functionalized polymers are relatively hydrophobic, which typically makes them dense in aqueous solutions and hinders the diffusion of uranyl ions into the adsorbent interior. Therefore, only the surface AO groups exhibit high uranium adsorption efficiency. The adsorbed uranyl ions form a cross-linked polymer layer, which decreases the free volume of the

adsorbent and blocks the diffusion channels for subsequent uranyl ions. Thus, the utilization of the AO groups in adsorbents has remained below 1/100 for decades [28].

An effective strategy for increasing the adsorption capacity and simultaneously accelerating the adsorption rate of AO-based adsorbents is to considerably increase the specific surface area of the adsorbents [29, 30] by fabricating ultrathin, ultrafine, and microporous structures. Many new materials have been fabricated for uranium extraction, including covalent organic frameworks (COFs), metal organic frameworks, and porous organic polymers [31]. Wen et al. prepared a new graphene-synergized 2D COF-based composite (o-GS-COFs) with AO groups, which reached a maximum uranium adsorption capacity of 220.1 $mg \cdot g^{-1}$ under acidic conditions [32]. Although these materials have the advantages of a large specific surface area and high adsorption capacity, their structural affinity and strength are weak, and they easily collapse or hydrolyze, making it difficult to prepare them cost-effectively on a large scale [33]. This uneconomical large-scale preparation of adsorption materials negatively affects the strategic importance of uranium extraction from seawater. Overcoming these limitations requires the development of efficient, durable, and low-cost AO adsorbents.

Here, we report a novel technology for introducing a branched adsorption layer (HBP) containing AO groups onto a fiber surface with a high utilization rate of the AO group. This new strategy maintains the mechanical strength of the trunk fiber while improving the free volume of the adsorption layer, resulting in materials with long-term service and significant adsorption properties. Nitrile groups can be immobilized on the polypropylene/polyethylene spun-laced nonwoven (PP/PE SNW) fiber surface via a combination of RIGP and a series of chemical modifications: the (1) introduction of epoxy groups via the RIGP of glycidyl methacrylate (GMA; P-GMA), (2) immobilization of the hyperbranched structure via the reaction of amino and epoxy (P-HBP), (3) anchoring of AN via the addition reaction (P-HBP-AN), and (4) amidoximation of the nitrile groups to obtain AO (P-HBP-AO). To overcome the limitation of ion diffusion channel blockage caused by AO group cross-linking due to uranium adsorption, we propose a new process for preparing uranium adsorption materials.

2. Methodology (Design/Approach)

2.1. Materials

PP/PE SNW ($30 g \cdot m^{-2}$) fibers were purchased from HLB New Material Technology Co., Ltd., Dalian China. GMA was purchased from Shanghai Aladdin Biochemical Technology Co., Ltd. Polyethyleneimine (PEI), AN, and uranium standard solutions were purchased from Joye Chemical Co., Ltd., Guangdong, China. Tween 80, 1,4-dioxane, hydroxylamine hydrochloride, hydrochloric acid, sodium hydroxide, potassium hydroxide, acetone, dimethyl sulfoxide (DMSO), and anhydrous

ethanol were purchased from WAK-Chemie Medical GmbH Co., Ltd., Germany. The reagents were not purified before use. All experiments used ultrapure water (UPW), unless otherwise noted.

2.2. Preparation of P-HBP-AO adsorbents

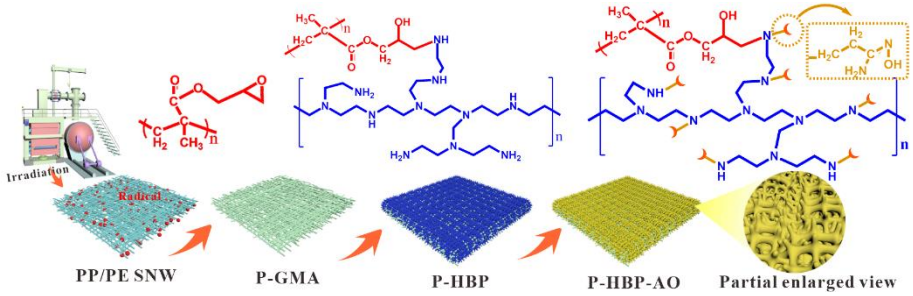

Scheme 1. Schematic of the fabrication process and chemical structure of P- HBP-AO

The P-HBP-AO adsorbents with functionalized AO groups for uranium adsorption at low concentrations were fabricated using the procedure shown in Scheme 1. The detailed conditions for the emulsion graft polymerization of GMA, including the adsorption dose, monomer concentration, graft time, and temperature, have been described previously [34]. Transferred into a Soxhlet extractor, the grafted PP/PE SNW (nominated as P-GMA) fiber was extracted with acetone for roughly 24 h to remove any remaining monomers and homopolymers before being dried at 60 °C in a vacuum oven until constant weight. We used Eq. (1). to determine the DG.

$$DG(\%) = \frac{W_1 - W_0}{W_0} \times 100 \quad (1)$$

where W_0 and W_1 represent the PP/PE SNW fiber weights before and after graft polymerization, respectively. Grafted nonwoven fabric with a DG of 20% was used in this study.

The grafted chain epoxy groups and the amino group of the branched PEI engaged in a ring-opening reaction to introduce PEI onto the surface of the PP/PE SNW fiber. P-GMA (2.0 g) was placed in a 300-mL wide-mouth conical flask containing PEI (50 g) and 1,4-dioxane (150 mL). After purging the solution with N_2 for 15 min to remove O_2, the conical flask was sealed before commencing the reaction at 80 °C for 4 h. Thereafter, the amination product was thoroughly cleaned to remove the remaining PEI and solvent by using ethanol solution and UPW and then dried in a vacuum oven at 60 °C. The resulting product was termed P-HBP. Graft chains containing AN and P-HBP were submerged in a 20% (v/v) AN/ethanol solution at 40 °C for 4 h, using the Michael addition reaction between AN and amine groups. The addition product was termed P-HBP-AN. It was washed

several times with an ethanol solution and UPW to remove the remaining AN and solvent and then dried in a vacuum oven at 60 °C. In a DMSO/H_2O (v/v = 1:1) solution, hydroxylamine hydrochloride was reacted for 2 h at 80 °C and pH 7.0. The sample was then removed from the reaction solution and repeatedly rinsed with UPW. The collected sample was designated P-HBP-AO.

The obtained sample was denoted as P-HBP-AO. The density of the AO group was evaluated using Eq. (2):

$$AO\ Density(mmol \cdot g^{-1}) = \frac{1000(W_3 - W_2)}{32.9W_3} \quad (2)$$

where 32.9 is the molecular weight of the amino and hydroxyl groups, and W_2 and W_3 are the weights of P-HBP-AN and P-HBP-AO, respectively. The resulting P-HBP-AO had an AO group density of 1.78 mmol·g^{-1}.

2.3. Characterization

A Fourier-transform infrared (FT-IR) spectrophotometer (TJGD iS50, China) was used to detect changes in the chemical structures of the materials. The spectra were captured between 350 and 7500 cm^{-1} with a 4-cm^{-1} resolution.

The chemical compositions of the pristine and modified PP/PE SNW fibers were determined using X-ray photoelectron spectroscopy (XPS, with Kratos, England). As a benchmark, the C1s peak at 285.0 eV was chosen.

A scanning electron microscope (SEM, CIQTEK, China) was used to observe the morphologies of the unaltered and altered PP/PE SNW fibers at an acceleration voltage of 10 kV. A gold layer (approximately 10 nm) was sputter-coated onto the samples.

A thermogravimetric analyzer (TGA, NETZSCH, Germany) was used for analysis from 25 to 800 °C under an N_2 atmosphere with a heating and flow rate of 10 °C·min^{-1} and 30 mL·min^{-1}, respectively.

An optical contact angle measuring instrument (OCAM, T301, Germany) was used to test the hydrophilic performance using 2 × 4 cm sample strips of PP/PE SNW fibers before and after modification, and the outcomes of each experiment were averaged after five runs.

2.4 Adsorption tests

The adsorption properties of P-HBP-AO toward a low concentration of uranium in aqueous solution were analyzed using a batch adsorption process. Subsequently, 50 mg of P-HBP-AO was mixed with 100 mL uranium solution (approximately 500 μg·L^{-1}) in a 150-mL wide-mouth polypropylene bottle. The pH of the solution was adjusted using negligible volumes of NaOH and HCl. At 25 °C, the adsorption solution was stirred at 120 rpm in a thermostatic oscillator (NTS-

4000C, Japan). Inductively coupled plasma mass spectrometry (ICP-MS, with ELEMENT 2, USA) and inductively coupled plasma optical emission spectrometry (ICP-OES, with Optima 8000, USA) were used to measure the uranyl ion concentrations in the solutions.

Eq. (3) was used to determine the uranium removal rate (%).

$$Removal\ ratio(\%) = \frac{C_0 - C_e}{C_e} \times 100 \quad (3)$$

where C_0 is the initial uranium concentration and C_e is the equilibrium uranium concentration ($mg \cdot L^{-1}$).

3. Results

3.1. Design of P-HBP-AO

The low utilization of AO groups is a critical limitation of AO-based uranium adsorbents because it prolongs the process of reaching adsorption equilibrium, reduces the adsorption capacity, and increases the cost of technology. Therefore, the development of improved uranium-binding materials that are selective and have high ligand utilization rates is crucial for enhancing the efficiency of uranium extraction from natural seawater. To address this issue, we designed a branched functional layer on PP/PE SNW fiber surface. Commercially available branched PEI was anchored to the PP/PE SNW fiber surface and chemically modified to obtain an AO-based adsorbent. Branched PEI was selected based on the following considerations. First, PEI is super hydrophilic, which significantly improves the swelling degree of the adsorbents in water and improves the adsorption rate of uranyl ions. Second, compared with linear analogs, branched structures possess considerable free volume and weak intermolecular forces, which are conducive to ion diffusion. Third, numerous terminal adsorptive groups enable a wide scope for chemical modification, and the distribution of ligands along the peripheries of the dendrites increases the effective utilization of the ligands. The branched structure and facile chemical modification of the adsorbents developed in this study fulfill the criteria for sustainable high ligand utilization materials.

3.2. Characterization of modified PP/PE SNW fibers

3.2.1. FT-IR and XPS spectra

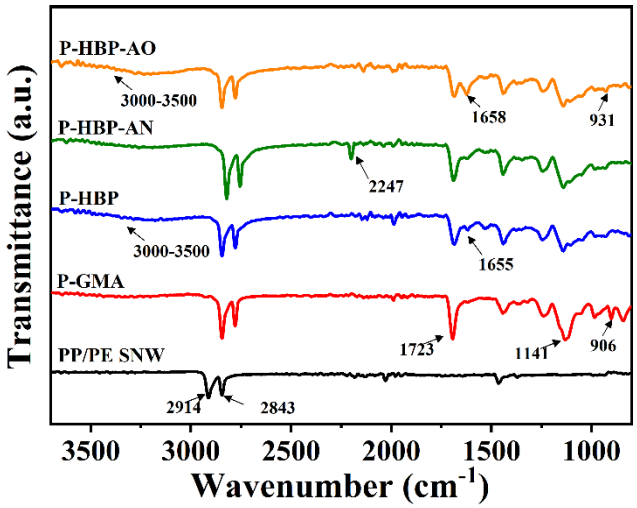

Fig. 1. FT-IR spectra of PP/PE SNW, P-GMA, P-HBP, P-HBP-AN, and P-HBP-AO.

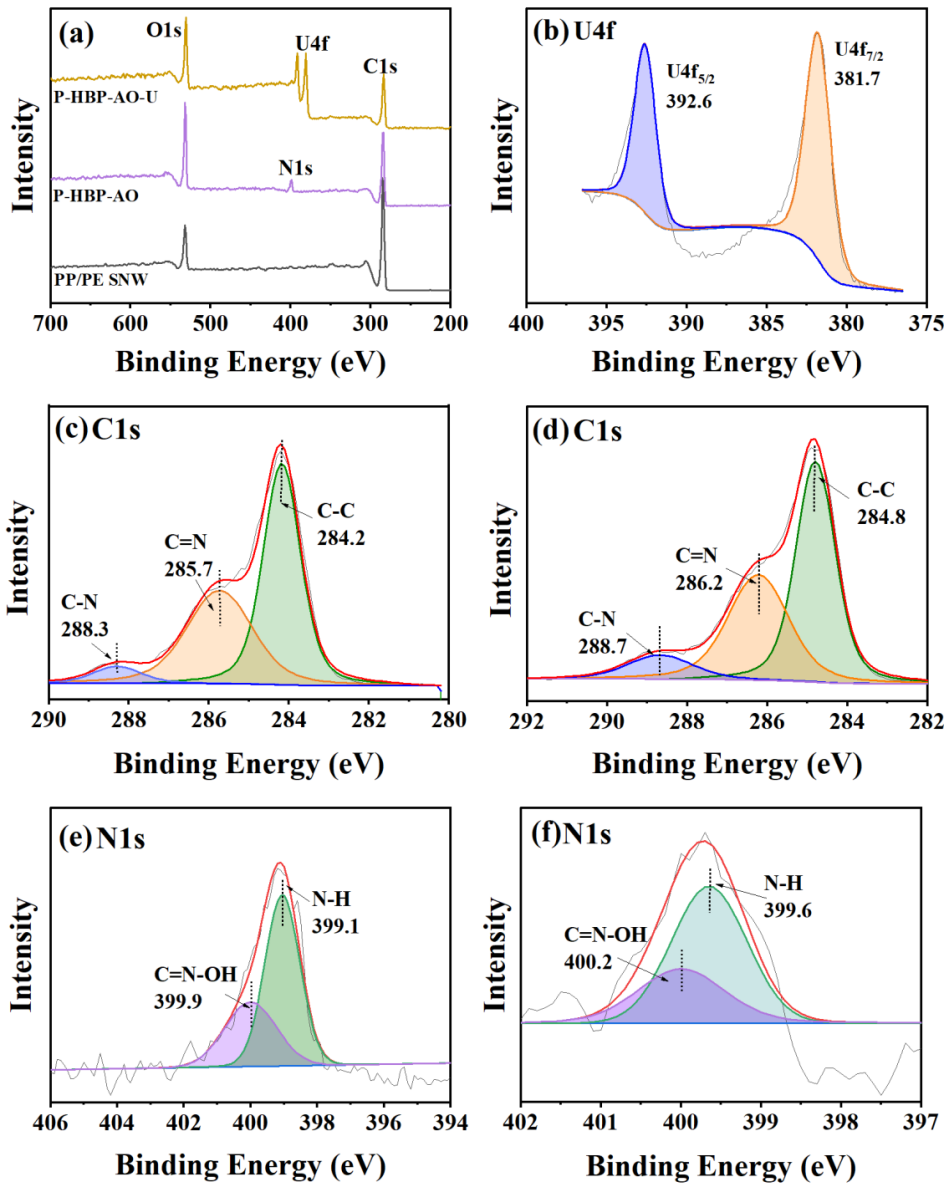

Fig. 2. (a) XPS spectra of PP/PE SNW, P-HBP-AO, and P-HBP-AO-U. (b) U4f spectrum of P-HBP-AO-U. C1s spectra of P-HBP-AO before (c) and after (d) adsorption. N1s spectra of P-HBP-AO before (e) and after (f) adsorption.

Variations in the chemical structures of the PP/PE SNW fibers induced through grafting and chemical modification (Fig. 1) were validated by the FT-IR spectra. Compared with the spectrum of the pristine fabric, the spectrum of P-GMA shows three additional peaks assigned to the epoxy group (906 cm^{-1}) [35], -C-O (1141 cm^{-1}) [36], and -C=O (1723 cm^{-1}) [37], indicating that GMA, which contains abundant epoxy groups, was anchored to the PP/PE SNW fiber via chemical bonding. By contrast, the epoxy group peaks were not present in the P-HPB spectrum, and the additional peaks at 1655 and

3000–3500 cm^{-1} contributed to the N-H vibration in PEI, confirming the successful ring-opening reaction of the epoxy groups. A -C≡N stretching vibration is visible at 2247 cm^{-1} [38], indicating that the nitrile group was smoothly introduced into the trunk of the PP/PE SNW fiber. The disappearance of the -C≡N at 2247 cm^{-1} and the presence of -NH_2-OH (3000–3500 cm^{-1}), C=N (1658 cm^{-1}), and N-O (1658 cm^{-1}) peaks in the P-HBP-AO spectrum confirms the translation of nitrile groups into AO groups. These results demonstrate that all modification steps were successful and that P-HBP-AO was successfully fabricated.

The XPS spectra of the PP/PE SNW, P-HBP-AO, and P-HBP-AO-U were obtained to study further changes in the chemical structures (Fig. 2). The typical signals of C1s, N1s, and O1s are represented by peaks at 284.5, 399.1, and 532.0 eV, respectively. (Fig. 2a). After uranium adsorption, the P-HBP-AO-U spectrum contained the characteristic U4f peaks, indicating that uranyl ions were successfully adsorbed by the sample. The U4f absorption energy spectrum of P-HBP-AO-U was deconvoluted into two peaks, $U4f_{7/2}$ (381.7 eV) and $U4f_{5/2}$ (392.6 eV), both of which correspond to U(VI), indicating that uranium adsorbed on P-HBP-AO-U was present in the hexavalent form (Fig. 2b). The C1s and N1s energy spectra of P-HBP-AO were deconvoluted, and the results are shown in Figs. 2c–f. The C1s peaks centered at 284.2, 285.7, and 288.3 eV can be assigned to the typical peaks of C-C, C-N, and C=N, respectively [39]. The N1s peaks centered at 399.1 eV and 399.9 eV could be assigned to C=N and N-H [40]. In addition, the C=N and N-H peaks in the P-HBP-AO-U sample shift from 399.1 to 399.6 eV and 399.9 to 400.2 eV, respectively. This shift is due to the decrease in the electron cloud density around the N atom after uranium adsorption, which causes the C=N and N-H of the AO groups to move toward a higher binding energy, indicating that adsorption on P-HBP-AO occurs via coordination of the AO groups with uranium.

3.2.2 scanning electron microscopy (SEM) for surface morphology analyses

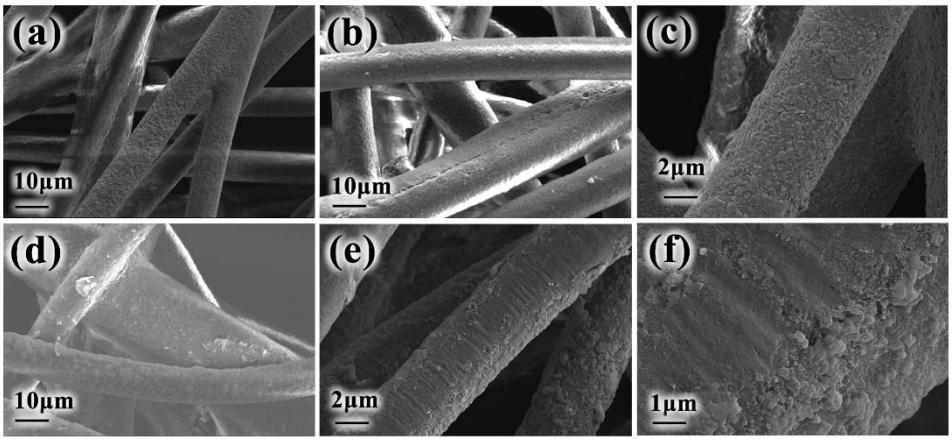

Fig. 3. SEM images of (a) PP/PE SNW, (b) P-GMA, (c)P-HBP, (d) P-HBP-AO, (e) and (f) P-HBP-

AO-U.

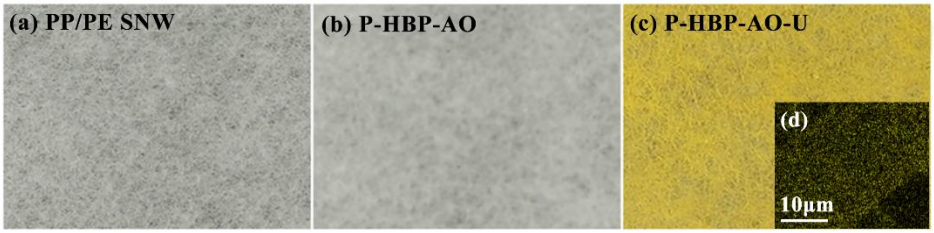

Fig. 4. Images of pristine (a) PP/PE SNW, (b) P-HBP-AO, and (c) P-HBP-AO-U after uranium adsorption. (d) EDS mapping image of uranium.

The morphologies of pristine PP/PE SNW, P-GMA, P-HBP, P-HBP-AO, and P-HBP-AO-U were characterized using SEM. As shown in Fig. 3a–f, the modified surfaces are rough and granular, in contrast with the smooth surface of the pristine fabric. Moreover, the average diameters of the fibers significantly increased after grafting polymerization and three-step modification, implying that radiation grafting and chemical modifications proceeded successfully with no obvious damage observed during preparation. The color of P-HBP-AO also changed noticeably after adsorption, from light gray to medium yellow (Fig. 4), indicating a high concentration of uranium on P-HBP-AO.

3.2.3 TG for thermal stability analysis

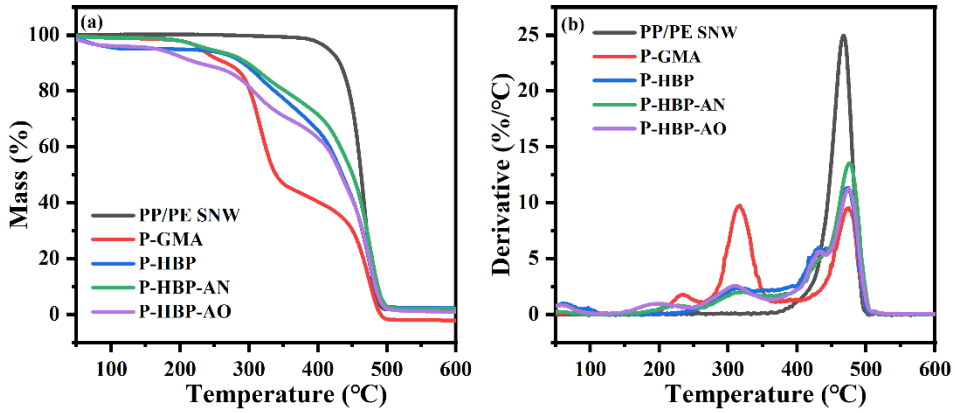

Fig. 5. TG (a) and DTG (b) curves of pristine and modified PP/PE SNW fibers.

The thermal stabilities of the pristine and modified fabrics were tested using TG under a nitrogen atmosphere, and the results are presented in Fig. 5. The pristine fabric curve shows a one-step degradation, while the decomposition temperature is 467 °C. By contrast, the thermal degradation of modified fabrics can be divided into multistep degradation patterns based on the derivative TG (DTG) curves. The degradation of the grafted chains occurs below 420 °C because of their amorphous morphology and low molecular weight. The final step is a domain degradation stage at approximately 470 °C, which is the same as that of the pristine fabric. The thermal stability decreased after the modification. However, the modified materials still possessed high thermal stability and no negative effects were observed during normal adsorption applications.

3.2.4 Contact angle measurement for hydrophilicity analysis

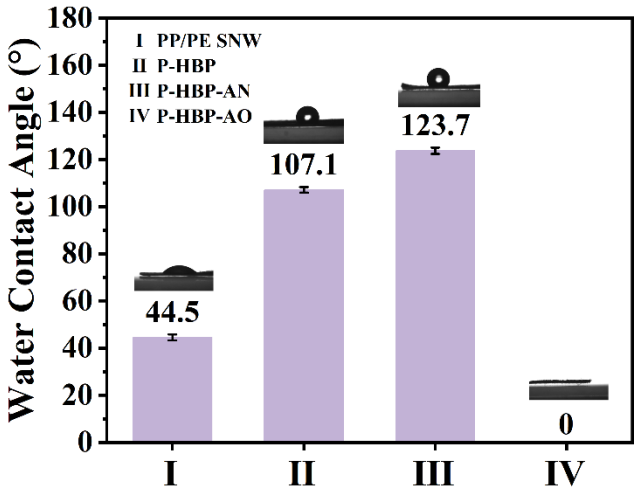

Fig. 6. Water contact angle for PP/PE SNW, P-HBP, P-HBP-AN, and P-HBP-AO

The surface hydrophilicity of the adsorbent significantly influences its adsorption performance because it affects the free volume of the adsorbent and the possibility of contact between the adsorption group and the target ion, which determines the diffusion rate and adsorption capacity. The water wettability of the pristine and modified fabrics was characterized using contact angle measurements. As shown in Fig. 6, each chemical modification step has a significant influence on the surface characteristics of the material (conversion between hydrophilicity and hydrophobicity), confirming successful chemical modification. After the final amidoximation, the contact angle of P-HBP-AO decreased to zero owing to the superhydrophilicity of the AO groups. A low contact angle is conducive to the adsorption of metal ions by the adsorption materials.

3.3 Effect of pH on uranium adsorption

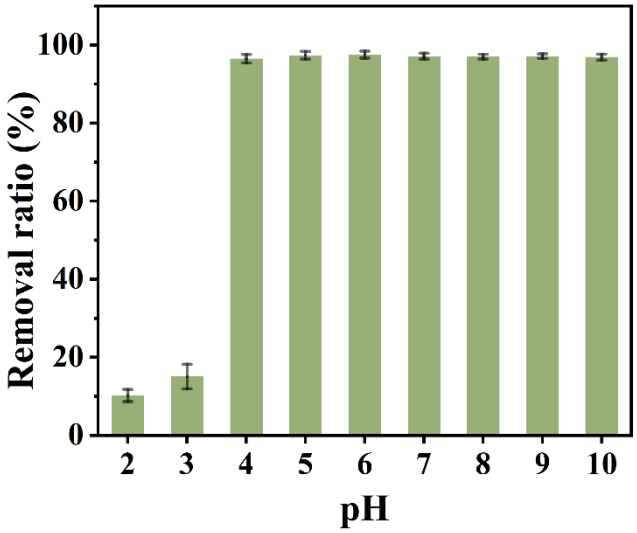

Fig. 7. Effect of pH on uranium removal by P-HBP-AO.

For pH determines U(VI) species and influence the charge distribution on the adsorbent surface, the uranium adsorption performance of P-HBP-AO at different pH values was investigated. Batch adsorptions were implemented in the pH range of 2–10 at 25 ℃ for 24 h with 500 $\mu g \cdot L^{-1}$ uranium and 50 mg P-HBP-AO. The uranium removal ratios at various pH values are shown in Fig. 7. When the pH was 2 or 3, abundant H^+ ions competed with uranyl for the binding sites on P-HBP-AO, leading to low U(VI) removal ratios [41]. In the pH range of 4–10, the uranium removal ratio of P-HBP-AO reached 98.2% and remained stable, in contrast with the results reported for other AO-based adsorbents [42-44], indicating that the PEI-AO group has a strong coordination ability with uranium species and a wide pH range [45]. Uranyl ions typically exhibit complex structures at different pH values. In acidic solutions, uranium ions exist as UO_2^{2+}, whereas $(UO_2)_3(OH)_5^+$ is the dominant species at a pH 5–8. When the pH was higher than 8, uranium mainly existed as negative ions, namely, $(UO_2)_3(OH)_7^-$ and $UO_2(OH)_3^-$. The high adsorption capacity over a wide pH range may be attributed to the unique hyperbranched structure and functional group distribution of P-HBP-AO. Nitrogen atoms in the branched structure can adjust the electron cloud distribution of AO groups, forming a synergistic adsorption effect [46]. Similar results were demonstrated in a study on the removal of uranyl ions from fluorinated radioactive wastewater by using AO groups [47]. Because the main uranium species at pH 4 is UO_2^{2+}, which is the major uranium (VI) species in seawater [48], pH 4 was selected as the optimal pH for subsequent adsorption studies. Unless otherwise stated, all adsorption experiments were conducted at this value.

3.4 Adsorption kinetics

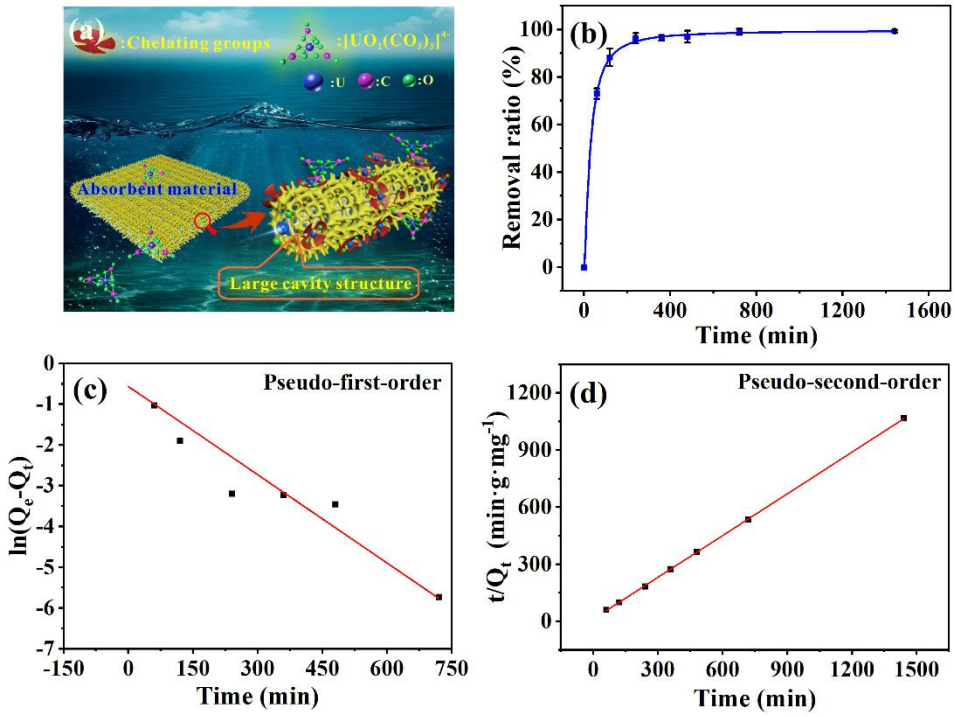

Fig. 8. (a) Branched structure of P-HBP-AO. (b) Removal ratio varied with adsorption time. (c) Pseudo-first-order and (d) pseudo-second-order models for uranium removal by P-HBP-AO

The rapid removal of uranium from water reveals the high efficiency of the adsorbent, which is conducive to saving time and minimizing costs in actual applications. The time dependence of the uranium removal ratio was evaluated at pH 4 and 25 °C (Fig. 8a). Compared with reported uranium adsorption materials [49-52], P-HBP-AO exhibited an ultrafast adsorption rate for uranyl ions, with uranium removal ratios of 73.0% and 88.2% after 60 and 120 min, respectively. The adsorption rate gradually decelerated with an increase in time owing to the decreasing number of uranium and unoccupied adsorption sites and finally plateaued. The uranium removal ratio reached 96.3% within 240 min, and the residual uranium concentration was approximately 18.7 μg·L^{-1}. The residual concentration of uranium was less than 5 μg·L^{-1} in 12 h, illustrating that the uranium removal ratio within 12 h was close to 100%.

Research on adsorption kinetics is important to fully understand the adsorption process. Pseudo-first-order and pseudo-second-order kinetic models were adopted to simulate the adsorption kinetics, as given in Eqs. (4) and (5), respectively.

$$\ln(Q_e - Q_t) = \ln Q_e - k_1 t \quad (4)$$

$$\frac{t}{Q_t} = \frac{t}{Q_e} + \frac{1}{k_2 Q_e^2} \quad (5)$$

where Q_e (mg·g^{-1}) and Q_t (mg·g^{-1}) are the uranium adsorbed on P-HBP-AO at equilibrium time and t (min), and k_1 (min^{-1}) and k_2 (g·mg^{-1}·min^{-1}) are the adsorption kinetic constants for pseudo-first-order and pseudo-second-order kinetic adsorption, respectively. The simulation results are displayed in Fig. 8c and d. The kinetic parameters are listed in Table 1. The coefficient of determination (R^2) for the pseudo-second-order adsorption model was closer to 1 than that of the pseudo-first-order adsorption model, indicating that the data fits the pseudo-second-order model better. These results indicate that chemical adsorption plays a pivotal role in determining the U(VI) adsorption rate.

Table 1. Kinetic parameters for uranium adsorption by P-HBP-AO

Pseudo-first-order adsorption model			Pseudo-second-order adsorption model		
$k_1 \times 10^{-3}$ (min^{-1})	Q_e (mg·g^{-1})	R_1^2	k_2(g·mg^{-1}·min^{-1})	Q_e (mg·g^{-1})	R_2^2
7.220	0.570	0.9071	0.045	1.368	0.9999

3.5 Adsorption isotherms

Adsorption isotherm experiments were performed to assess the maximum uranium adsorption capacity of the P-HBP-AO adsorbent (uranium concentration 2–100 mg·L^{-1}, pH 4, and adsorption time of 24 h). The equilibrium adsorption capacity (Q_e) varied with the equilibrium uranium concentration (C_e) in the solution (Fig. 9a). The adsorption isotherm data shows that, as C_0 increased, the amount of uranium adsorbed onto P-HBP-AO gradually increased and finally plateaued, indicating that P-HBP-AO reached its maximum adsorption capacity. To calculate the maximum uranium adsorption capacity, the experimental data were simulated using the Langmuir and Freundlich isotherm adsorption models [53], given in Eqs. (6) and (7), respectively. The fitted data are shown in Figs. 9b and c.

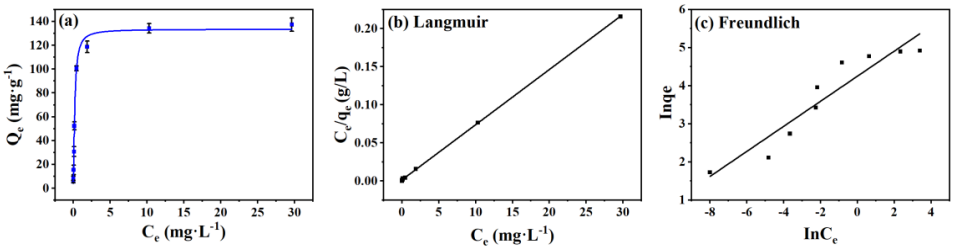

Fig. 9. (a) Adsorption isotherm of P-HBP-AO for uranium. (b) Langmuir and (c) Freundlich isotherms for uranium adsorption by P-HBP-AO.

The Langmuir and Freundlich equations are as follows:

$$\frac{C_e}{Q_e} = \frac{1}{bQ_m} + \frac{C_e}{Q_m} \quad (6)$$

$$ln\, Q_e = ln\, K_F + \left(\frac{1}{n}\right) ln\, C_e \quad (7)$$

where b is the Langmuir constant, which represents the affinity of adsorbent to uranium [54]; Q_e, C_e, and Q_m are the equilibrium adsorption capacity of P-HBP-AO ($mg \cdot g^{-1}$), the equilibrium concentration in solution ($mg \cdot L^{-1}$), and the maximum adsorption capacity of P-HBP-AO ($mg \cdot g^{-1}$), respectively. K_F is the adsorption constant, and 1/n is the adsorption intensity. The corresponding parameters are listed in Table 2.

Table 2. Isotherm adsorption parameters for uranium adsorbed on P-HBP-AO.

Langmuir			Freundlich		
Q_m ($mg \cdot g^{-1}$)	b ($L \cdot mg^{-1}$)	R_L^2	K_F	1/n	R_F^2
138.12	4.993	0.9998	70.10	3.04	0.8937

The fitting parameter of the Langmuir model (R_L^2= 0.9998) was higher than that of the Freundlich model (R_F^2=0.8937), demonstrating that the Langmuir isothermal adsorption model is applicable to uniform chemical adsorption and is in accordance with the uranium adsorption behavior of the P-HBP-AO adsorbent. The maximum adsorption capacity Q_m (138.12 $mg \cdot g^{-1}$) derived from the Langmuir model corresponds well with the experimental Q_e (137.33 $mg \cdot g^{-1}$). This result confirms the high rate of AO utilization on the adsorbent surface.

The rate of AO utilization, described as the molar ratio of uranium to AO groups, was calculated according to Eq. 8.

$$R = \frac{m_u}{m_{AO}} \quad (8)$$

where m_u is the capacity of uranium (mmol·g^{-1}) adsorbed by P-HBP-AO, and m_{AO} is the AO concentration (mmol·g^{-1}) of P-HBP-AO. A higher R value indicates a higher AO utilization ratio [3]. The structures of the primary (RNH_2) and secondary amines (R_2NH) have been reported to affect the adsorption of uranyl ions. To investigate whether RNH_2 and R_2NH affect the adsorption of uranium by P-HBP-AO, 50 mg P-HBP-AN was immersed in a 500 μg·L^{-1} solution of uranium ions at pH 4 at 25 °C. The residual uranium ion concentration in the solution was measured after 24 h using inductively coupled plasma mass spectrometry. These results were used to verify the transformation of RNH_2 and R_2NH in the branched-chain structure during AN addition. The uranium removal ratio of P-HBP-AN was <3% after 24 h, indicating that the conversion rate in the addition reaction between P-HBP and -AN was complete, with minimal residual RNH_2 and R_2NH groups in the branched graft chains of P-HBP-AN. Therefore, during the adsorption process, only the AO groups of P-HBP-AO contributed to the adsorption behavior, with AO utilization calculated using Eq. 8. The AO utilization ratio of P-HBP-AO was 1/3.5, indicating that 3.5 adsorption groups captured only one uranyl ion. In summary, in the solution with a uranium concentration of 500 μg·L^{-1}, the maximum monolayer adsorption capacity at 25 °C was 138.12 mg·g^{-1}. Notably, the maximum AO utilization rate reached 1/3.5, which was significantly higher than the previously reported value [55-57].

The distribution coefficient (K_d, mL·g^{-1}) is a critical indicator for the affinity between adsorbent and metal ions and is obtained using Eq. (9).

$$K_d = \frac{C_0 - C_e}{C_e} \times \frac{V}{m} \quad (9)$$

where C_0 (mg·L^{-1}) and C_e (mg·L^{-1}) represent the initial and adsorption equilibrium uranium concentrations, and V (mL) and m (g) represent the volume of the solution and weight of the adsorbent, respectively.

K_d values for the P-HBP-AO adsorbent were 2.82×10^6, 9.02×10^5, 4.72×10^5, and 2.18×10^5 mL·g^{-1} with the initial uranium concentrations of 2, 10, 25, and 50 mg·L^{-1}, respectively. Typically, the K_d value of a good adsorbent is above 1.0×10^4 mL·g^{-1} [58]. P-HBP-AO exhibited high K_d values, indicating a strong affinity for uranyl ions. This result was confirmed using energy-dispersive spectroscopy mapping (Fig. 4d), which showed a high concentration of uniformly distributed uranium on the P-HBP-AO surface after adsorption.

3.6 Adsorption selectivity

Selective adsorption tests at various solid-to-liquid ratios (the adsorbent mass to solution volume) were conducted in an aqueous solution containing multiple heavy metal ions for 12 h (25 ℃, pH 4) to verify the remarkable selectivity and affinity of P-HBP-AO for uranium. The concentration of UO_2^{2+} in the aqueous solution was 500 μg·L^{-1}, and the concentrations of V^{5+}, Pb^{2+}, Cu^{2+}, Mn^{2+}, Zn^{2+}, Ni^{2+}, and Co^{2+} were all 5 mg·L^{-1}. Adsorption ratios of U, Mn, and V were measured using ICP-MS, and of other metal ions were measured using ICP-OES. The results were calculated using Eq. (3) and are presented in Fig. 10.

P-HBP-AO shows high selectivity and affinity for uranium at various solid-to-liquid ratios. Uranium has a substantially higher adsorption capability than the majority of the other metal ions (Pb^{2+}, Cu^{2+}, Zn^{2+}, Mn^{2+}, Ni^{2+}, and Co^{2+}). An exception was vanadium, which exhibited adsorption levels similar to those of uranyl ions at certain solid-to-liquid ratios. Vanadium is the most competitive ion for uranium extraction from seawater because it strongly complexes with AO fibers and is difficult to elute. However, the selectivity of the adsorbent was higher toward uranyl ions than toward vanadium ions at an initial concentration of only one-tenth that of the vanadium ions, which indicates a higher adsorption selectivity for uranium. This outstanding selectivity demonstrates the potential of these adsorbents for large-scale extraction of uranium from seawater. Although this study focused on a 24-h adsorption period, the removal rate was still greater than 88.2% and increased slightly (89.9%) with an increase in the solid-to-liquid ratio from 0.1 to 1.0 g·L^{-1}.

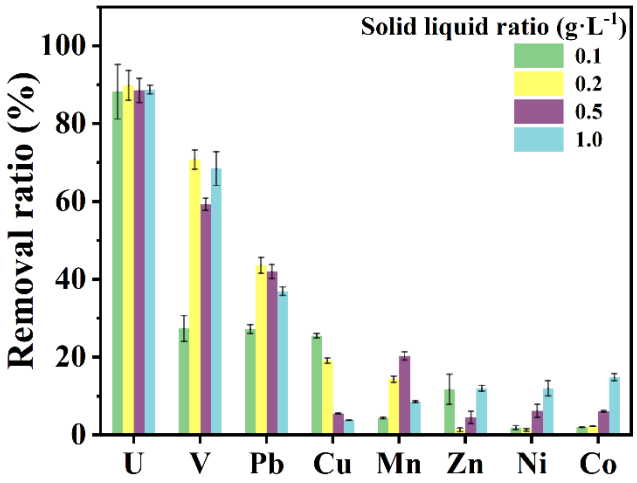

Fig. 10. Adsorption selectivity of P-HBP-AO for uranium.

3.7 Regeneration studies

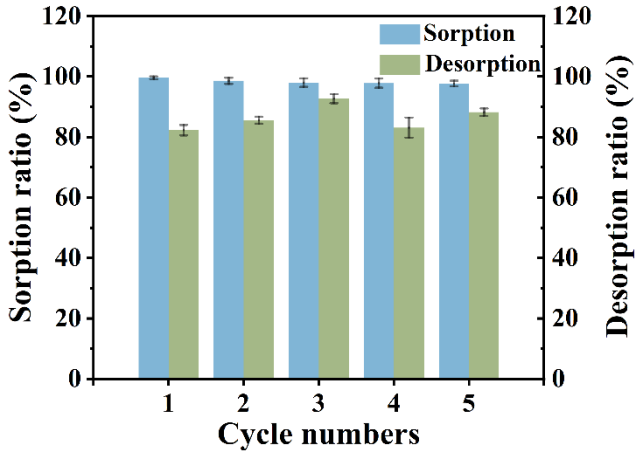

Fig. 11. Desorption and reusability of P-HBP-AO for uranium.

Desorption experiments are important for studying the regeneration of P-HBP-AO from an economic perspective. The reusability of the adsorbent was examined over five adsorption–desorption cycles. An HCl solution with a concentration of 1 mol·L^{-1} was used to achieve the desorption process, which was conducted for 3 h per cycle. After desorption, the P-HBP-AO was deprotonated with 0.44 mol·L^{-1} KOH solution at 80 °C. The adsorption rate remained high at 97.7%, and the desorption rate remained above 83%, reaching a maximum value of approximately 93% over five cycles (Fig. 11). These results indicate that P-HBP-AO exhibited excellent regeneration and reusability.

4. Discussion and conclusion

In this study, we used a PP/PE SNW substrate to fabricate P-HBP-AO adsorbent materials with branched structures using RIGP and chemical modification and characterized their chemical structures, microscopic morphologies, and adsorption mechanisms via FT-IR, SEM, and XPS. The adsorption capacity of P-HBP-AO for uranyl ions was high (137.33 $mg \cdot g^{-1}$), the adsorption rate for uranyl ions was fast, the adsorption time was close to that of the adsorption equilibrium (240 min), and the regeneration and reuse of the adsorbent were accessible. The adsorption kinetics was determined using a pseudo-second-order kinetic process, and the adsorption isotherms followed the Langmuir isothermal adsorption model. During the adsorption process, the AO utilization rate of the material reached 1/3.5, and it performed extremely well in the pH range of 4–10, with a uranyl ion removal ratio higher than 98%. Selective studies showed that P-HBP-AO selectively adsorbs uranium under the interference of various metal ions, demonstrating its potential for industrial applications.

ACKNOWLEDGEMENTS

We gratefully acknowledge the financial support from the National Natural Science Foundation of China (Grant Nos. 11675247 and 22176194).

References

[1] H. Guo, P. Mei, J. Xiao, et al., Carbon materials for extraction of uranium from seawater. Chemosphere. **278**, 130411 (2021). https://doi.org/10.1016/j.chemosphere.2021.130411

[2] X. Li, Z. Liu, M. Huang, Purification of uranium-containing wastewater by adsorption: a review of research on resin materials. J. Radioanal. Nucl. Ch. **331**, 3043-3075 (2022). https://doi.org/10.1007/s10967-022-08370-6

[3] C. Huang, L. Xu, X. Xu, et al., Highly amidoxime utilization ratio of porous poly(cyclic imide dioxime) nanofiber for effective uranium extraction from seawater. Chem. Eng. J. **443**, 136312 (2022). https://doi.org/10.1016/j.cej.2022.136312

[4] Y.M. Khawassek, A.M. Masoud, M.H. Taha, et al., Kinetics and thermodynamics of uranium ion adsorption from waste solution using Amberjet 1200 H as cation exchanger. J. Radioanal. Nucl. Ch. **315**, 493-502 (2018). https://doi.org/10.1007/s10967-017-5692-1

[5] R. Qadeer, J. Hanif, M. Khan, et al., UPTAKE OF URANIUM IONS BY MOLECULAR-SIEVE. Radiochim. Acta. **68**, 197-201 (1995). https://doi.org/10.1524/ract.1995.68.3.197.

[6] C.W. Abney, R.T. Mayes, T. Saito, et al., Materials for the Recovery of Uranium from Seawater. Chem. Rev. **117**, 13935-14013 (2017). https://doi.org/10.1021/acs.chemrev.7b00355

[7] J. Ao, X. Xu, Y. Li, et al., Research progress in uranium extraction from seawater. J. Radiat. Res. Radiat. **37**, 26 (2019). CNKI:SUN:FYFG.0.2019-02-001

[8] T. Chen, K. Yu, C. Dong, et al., Advanced photocatalysts for uranium extraction: Elaborate design and future perspectives. Coordin. Chem. Rev. **467**, 214615 (2022). https://doi.org/10.1016/j.ccr.2022.214615

[9] M. Kanno, PRESENT STATUS OF STUDY ON EXTRACTION OF URANIUM FROM SEA-WATER. J. Nucl. Sci. Technol. **21**, 1-9 (1984). https://doi.org/10.1080/18811248.1984.9731004

[10] C.J. Leggett, F. Endrizzi, L. Rao, Scientific Basis for Efficient Extraction of Uranium from Seawater, II: Fundamental Thermodynamic and Structural Studies. Ind. Eng. Chem. Res. **55**, 4257-4263 (2016). https://doi.org/10.1021/acs.iecr.5b03688

[11] T. Sahyoun, A. Arrault, R. Schneider, Amidoximes and Oximes: Synthesis, Structure, and Their Key Role as NO Donors. Molecules. **24** (2019). https://doi.org/10.3390/molecules24132470

[12] A.Y. Zhang, T. Asakura, G. Uchiyama, The adsorption mechanism of uranium(VI) from seawater on a macroporous fibrous polymeric adsorbent containing amidoxime chelating functional group. React. Funct. Polym. **57**, 67-76 (2003). https://doi.org/10.1016/j.reactfunctpolym.2003.07.005

[13] J. Xiong, Y. Fan, F. Luo, Grafting functional groups in metal-organic frameworks for U(VI) sorption from aqueous solutions. Dalton T. **49**, 12536-12545 (2020). https://doi.org/10.1039/D0DT02088E

[14] F. Chi, S. Zhang, J. Wen, et al., Functional polymer brushes for highly efficient extraction of uranium from seawater. J. Mater. Sci. **54**, 3572-3585 (2019). https://doi.org/10.1007/s10853-018-3040-7

[15] X. Xu, L. Xu, J. Ao, et al., Ultrahigh and economical uranium extraction from seawater via interconnected open-pore architecture poly(amidoxime) fiber. J. Mater. Chem. A. **8**, 22032-22044 (2020). https://doi.org/10.1039/D0TA07180C

[16] R. Li, H. Ma, Z. Xing, et al., Synergistic effects of different co-monomers on the uranium adsorption performance of amidoximated polyethylene nonwoven fabric in natural seawater. Radioanal. Nucl. Ch. **315**, 111-117 (2018). https://doi.org/10.1007/s10967-017-5639-6

[17] R. Li, L. Pang, M. Zhang, et al., Preparation of polypropylene fibrous adsorbents for extraction of uranium from seawater by radiation grafting method. Nucl. Sci. Tech. **40**, 050301 (2017). 10.11889/j.0253-3219.2017.hjs.40.050301

[18] N. Tang, J. Liang, C. Niu, et al., Amidoxime-based materials for uranium recovery and removal. J. Mater. Chem. A. **8**, 7588-7625 (2020). https://doi.org/10.1039/C9TA14082D

[19] Z. Zhao, G. Cheng, Y. Zhang, et al., Metal-Organic-Framework Based Functional Materials for Uranium Recovery: Performance Optimization and Structure/Functionality-Activity Relationships. Chempluschem. **86**, 1177-1192 (2021). https://doi.org/10.1002/cplu.202100315

[20] R.-H. Ding, X. Xu, C. Huang, et al., Development of a Fibrous Adsorbent Prepared Via Green Vapor-Phase Grafting Polymerization for Uranium Extraction. Acs Omega. **6**, 29675-29684 (2021). https://doi.org/10.1021/acsomega.1c04048

[21] A.T. Naikwadi, B.K. Sharma, K.D. Bhatt, et al., Gamma Radiation Processed Polymeric Materials for High Performance Applications: A Review. Front. Chem. **10**, 837111 (2022). https://doi.org/10.3389/fchem.2022.837111

[22] M. Komatsu, T. Kawakami, J.-I. Kanno, et al., Two-Stage Grafting onto Polyethylene Fiber by Radiation-Induced Graft Polymerization and Atom Transfer Radical Polymerization. J. Appl. Polym. Sci. **115**, 3369-3375 (2010). https://doi.org/10.1002/app.31451

[23] T. Saito, S. Brown, S. Chatterjee, et al., Uranium recovery from seawater: development of fiber adsorbents prepared via atom-transfer radical polymerization. J. Mater. Chem. A. **2**, 14674-14681 (2014). https://doi.org/10.1039/C4TA03276D

[24] P. Loganathan, G. Naidu, S. Vigneswaran, Mining valuable minerals from seawater: a critical review. Environ. Sci-Wat. Res. **3**, 37-53 (2017). https://doi.org/10.1039/C6EW00268D

[25] X. Xu, H. Yang, Z.G. Khalil, et al., Bromocatechol conjugates from a Chinese marine red alga, Symphyocladia latiuscula. Phytochemistry. **158**, 20-25 (2019). https://doi.org/10.1016/j.phytochem.2018.10.026

[26] S. Xie, X. Liu, B. Zhang, et al., Electrospun nanofibrous adsorbents for uranium extraction from seawater. J. Mater. Chem. A. **3**, 2552-2558 (2015). https://doi.org/10.1039/C4TA06120A

[27] B. Zhang, X. Guo, S. Xie, et al., Synergistic nanofibrous adsorbent for uranium extraction from seawater. RSC Adv. **6**, 81995-82005 (2016). https://doi.org/10.1039/C6RA18785D

[28] H. Zhao, X. Liu, M. Yu, et al., A Study on the Degree of Amidoximation of Polyacrylonitrile Fibers and Its Effect on Their Capacity to Adsorb Uranyl Ions. Ind. Eng. Chem. Res. **54**, 3101-3106 (2015). https://doi.org/10.1021/ie5045605

[29] C. Tissot, G.M. Pooley, M.A. Hadadi, et al., A highly regenerable phosphate-based adsorbent for Uranium in seawater: Characterization and performance assessment using U-233 tracer. Sep. Sci. Technol. **57**, 388-407 (2022). https://doi.org/10.1080/01496395.2021.1917612

[30] C.J. Leggett, F. Endrizzi, L. Rao, Scientific Basis for Efficient Extraction of Uranium from Seawater, II: Fundamental Thermodynamic and Structural Studies. Ind. Eng. Chem. Res. **55**, 4257-4263 (2015). https://doi.org/10.1021/acs.iecr.5b03688

[31] Yang, H., Liu, Y., Chen, Z. et al. Emerging technologies for uranium extraction from seawater. Sci. China Chem. **65**, 2335–2337 (2022). https://doi.org/10.1007/s11426-022-1358-1

[32] Gu, H., Liu, X., Wang, S. et al. COF-Based Composites: Extraordinary Removal Performance for Heavy Metals and Radionuclides from Aqueous Solutions. Reviews Env.Contamination (formerly:Residue Reviews) **260**, 23 (2022). https://doi.org/10.1007/s44169-022-00018-6

[33] Cai, YW., Fang, M., Hu, BW. et al. Efficient extraction of U(VI) ions from solutions. Nucl. Sci. Tech. **34**, 2 (2023). https://doi.org/10.1007/s41365-022-01154-3

[34] E.-L. Burton, M. Woodhead, P. Coates, et al., Reactive grafting of glycidyl methacrylate onto polypropylene. J. Appl. Polym. Sci. **117**, 2707–2714 (2010). https://doi.org/10.1002/app.31085

[35] Q. Gao, J. Hu, R. Li, et al., Radiation synthesis of a new amidoximated UHMWPE fibrous adsorbent with high adsorption selectivity for uranium over vanadium in simulated seawater. Radiat. Phys. Chem. **122**, 1-8 (2016). https://doi.org/10.1016/j.radphyschem.2015.12.023

[36] X. Feng, L. Qiu, M. Zhang, et al., Preparation of amidoxime-based ultra-high molecular weight polyethylene fiber for removing uranium from fluorine-containing wastewater. Nucl. Sci. Tech. **43**, 020301 (2020). CNKI:SUN:HJSU.0.2020-02-003

[37] E. Rosenberg, G. Pinson, R. Tsosie, et al., Uranium Remediation by Ion Exchange and Sorption Methods: A Critical Review. Johnson Matthey Tech. **60**, 59-77 (2016). https://doi.org/10.1595/205651316X690178

[38] D. Wang, J. Song, J. Wen, et al., Significantly Enhanced Uranium Extraction from Seawater with Mass Produced Fully Amidoximated Nanofiber Adsorbent. Adv. Energy Mater. **8**, 180267 (2018). https://doi.org/10.1002/aenm.201802607

[39] J. Cui, L. Zhang, Metallurgical recovery of metals from electronic waste: a review. J. Hazard Mater. **158**, 228-256 (2008). https://doi.org/10.1016/j.jhazmat.2008.02.001

[40] S. Liu, Y. Yang, T. Liu, et al., Recovery of uranium(VI) from aqueous solution by 2-picolylamine functionalized poly(styrene-co-maleic anhydride) resin. J Colloid Interface Sci. **497**, 385-392 (2017). https://doi.org/10.1016/j.jcis.2017.02.062

[41] Xu, X., Ding, XJ., Ao, JX. et al. Preparation of amidoxime-based PE/PP fibers for extraction of uranium from aqueous solution. Nucl. Sci. Tech. **30**, 20 (2019). https://doi.org/10.1007/s41365-019-0543-0

[42] Y. Yue, R.T. Mayes, J. Kim, et al., Seawater uranium sorbents: preparation from a mesoporous copolymer initiator by atom-transfer radical polymerization. Angew Chem. Int. Ed. Engl. **52**, 13458-13462 (2013). https://doi.org/10.1002/anie.201307825

[43] Xu, L., Hu, JT., Ma, HJ. et al. Amidoxime-based adsorbents prepared by cografting acrylic acid with acrylonitrile onto HDPE fiber for the recovery of uranium from seawater. Nucl. Sci. Tech. **28**, 45 (2017). https://doi.org/10.1007/s41365-017-0198-7

[44] P. Liu, Q. Yu, Y. Xue, et al., Adsorption performance of U(VI) by amidoxime-based activated carbon. J. Radioanal. Nucl. Ch. **324**, 813-822 (2020). https://doi.org/10.1007/s10967-020-07111-x

[45] L. Pang, L. Zhang, J. Hu, et al., High-performance functionalized polyethylene fiber for the capture of trace uranium in water. J. Radioanal. Nucl. Ch. **314**, 2393-2403 (2017). https://doi.org/10.1007/s10967-017-5603-5

[46] He Y, Mu L, Wang M, et al. Efficient removal of trace uranium from nuclear effluents using irradiation-functionalized fibrous adsorbents with very high salt tolerance. Chem. Eng. J. **461** (2023). https://doi.org/10.1016/j.cej.2023.141978

[47] Sun, Q., Aguila, B., Perman, J. et al. Bio-inspired nano-traps for uranium extraction from seawater and recovery from nuclear waste. Nat. Commun. **9**, 1644 (2018). https://doi.org/10.1038/s41467-018-04032-y

[48] Zhang M, Yuan M, Zhang M, et al. Efficient removal of uranium from diluted aqueous solution with hydroxypyridone functionalized polyethylene nonwoven fabrics. Radiat. Phys. Chem. **171** (2020) https://doi.org/10.1016/j.radphyschem.2020.108742

[49] Z. Zeng, Y. Wei, L. Shen, et al., Cationically Charged Poly(amidoxime)-Grafted Polypropylene Nonwoven Fabric for Potential Uranium Extraction from Seawater. Ind. Eng. Chem. Res. **54**, 8699-8705 (2015).

https://doi.org/10.1021/acs.iecr.5b01852

[50] Z. Li, Q. Meng, Y. Yang, et al., Constructing amidoxime-modified porous adsorbents with open architecture for cost-effective and efficient uranium extraction. Chem. Sci. **11**, 4747-4752 (2020). https://doi.org/10.1039/D0SC00249F

[51] Hao M, Chen Z, Liu X, et al. Converging Cooperative Functions into the Nanospace of Covalent Organic Frameworks for Efficient Uranium Extraction from Seawater. CCS Chemistry. **4(7)**, 2294-2307(2022). https://doi.org/10.31635/ccschem.022.202201897.

[52] Hao M, Xie Y, Liu X, et al. Modulating Uranium Extraction Performance of Multivariate Covalent Organic Frameworks through Donor-Acceptor Linkers and Amidoxime Nanotraps. JACS Au. Jan **23**;3(1):239-251 (2023) https://doi.org/10.1021/jacsau.2c00614

[53] M. Zhang, Q. Gao, C. Yang, et al., Preparation of Amidoxime-Based Nylon-66 Fibers for Removing Uranium from Low-Concentration Aqueous Solutions and Simulated Nuclear Industry Effluents. Ind. Eng. Chem. Res. **55**, 10523-10532 (2016). https://doi.org/10.1021/acs.iecr.6b02652

[54] S. Liu, Y. Yang, T. Liu, et al., Recovery of uranium(VI) from aqueous solution by 2-picolylamine functionalized poly(styrene- co -maleic anhydride) resin. J. Colloid Interf. Sci. **497**, 385-392 (2017). https://doi.org/10.1016/j.jcis.2017.02.062

[55] M. Piechowicz, R. Chiarizia, S. Skanthakumar, et al., Leveraging Actinide Hydrolysis Chemistry for Targeted Th and U Separations using Amidoxime-Functionalized Poly(HIPE)s. Chemphyschem. **21**, 1157-1165 (2020). https://doi.org/10.1002/cphc.202000155

[56] X. Chen, C. Wan, R. Yu, et al., Fabrication of amidoximated polyacrylonitrile nanofibrous membrane by simultaneously biaxial stretching for uranium extraction from seawater. Desalination. **486**, 114447 (2020). https://doi.org/10.1016/j.desal.2020.114447

[57] X. Xu, H. Zhang, J. Ao, et al., 3D hierarchical porous amidoxime fibers speed up uranium extraction from seawater. Energy Environ. Sci. **12**, 1979-1988 (2019). https://doi.org/10.1039/C9EE00626E

[58] S. Ma, L. Huang, L. Ma, et al., Efficient uranium capture by polysulfide/layered double hydroxide composites. J. Am. Chem. Soc. **137**, 3670-3677 (2015). https://doi.org/10.1021/jacs.5b00762

Figure Legends

Scheme 1. Schematic of Fabrication Process and Chemical Structure of the P- HBP-AO.

Fig. 1. FT-IR spectra of PP/PE SNW, P-GMA, P-HBP, P-HBP-AN, and P-HBP-AO.

Fig. 2. (a) XPS spectra of PP/PE SNW, P-HBP-AO, and P-HBP-AO-U. (b) U4f spectrum of P-HBP-AO-U. C1s spectra of P-HBP-AO before (c) and after (d) adsorption. N1s spectra of P-HBP-AO before (e) and after (f) adsorption.

Fig. 3. SEM images of (a) PP/PE SNW, (b) P-GMA, (c)P-HBP, (d) P-HBP-AO, (e) and (f) P-HBP-AO-U.

Fig. 4. Images of pristine (a) PP/PE SNW, (b) P-HBP-AO, and (c) P-HBP-AO-U after uranium adsorption. (d) EDS mapping image of uranium.

Fig. 5. TG (a) and DTG (b) curves of pristine and modified PP/PE SNW.

Fig. 6. Water contact angle for PP/PE SNW, P-HBP, P-HBP-AN, and P-HBP-AO

Fig. 7. Effect of pH on uranium removal by P-HBP-AO.

Fig. 8. (a) Branched structure of P-HBP-AO. (b) Removal ratio varied with adsorption time. (c) Pseudo-first-order and (d) pseudo-second-order models for uranium removal by P-HBP-AO

Fig. 9. (a) Adsorption isotherm of P-HBP-AO for uranium. (b) Langmuir and (c) Freundlich isotherms for uranium adsorption by P-HBP-AO.

Fig. 10. Adsorption selectivity of P-HBP-AO for uranium.

Fig. 11. Desorption and reusability of P-HBP-AO for uranium.

……

Figures

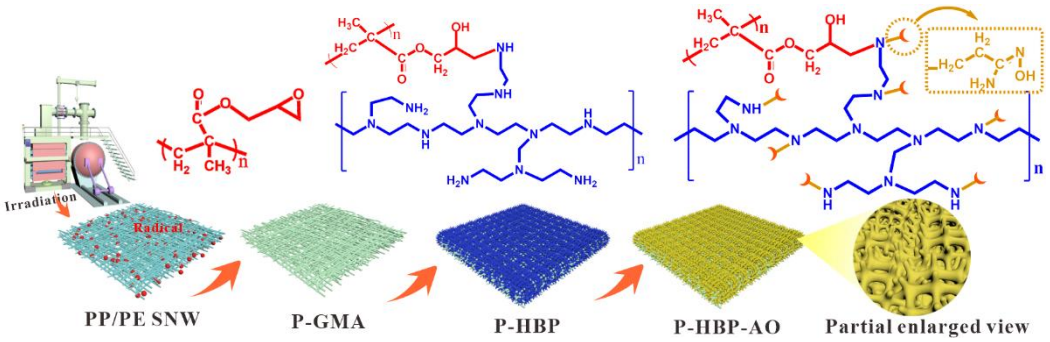

Scheme 1. Schematic of the fabrication process and chemical structure of P- HBP-AO

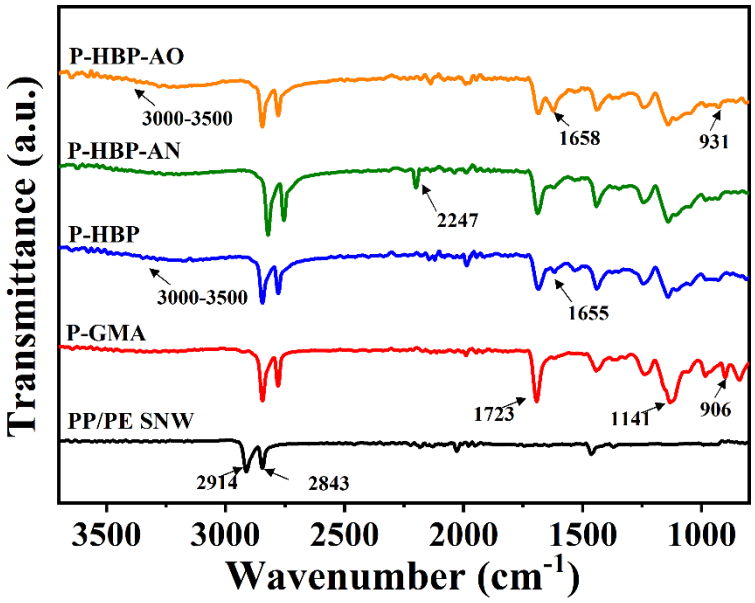

Fig. 1. FT-IR spectra of PP/PE SNW, P-GMA, P-HBP, P-HBP-AN, and P-HBP-AO.

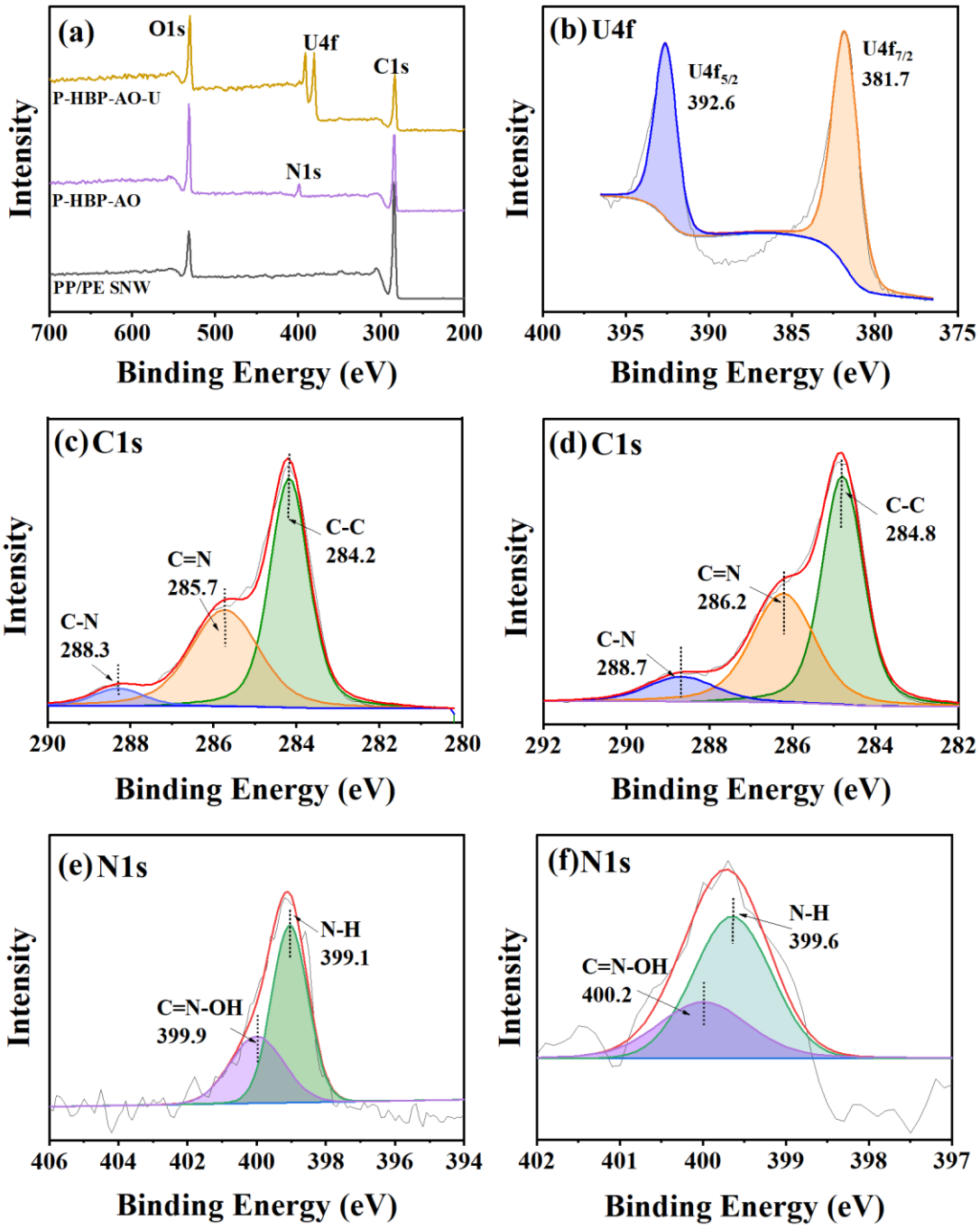

Fig. 2. (a) XPS spectra of PP/PE SNW, P-HBP-AO, and P-HBP-AO-U. (b) U4f spectrum of P-HBP-AO-U. C1s spectra of P-HBP-AO before (c) and after (d) adsorption. N1s spectra of P-HBP-AO before (e) and after (f) adsorption.

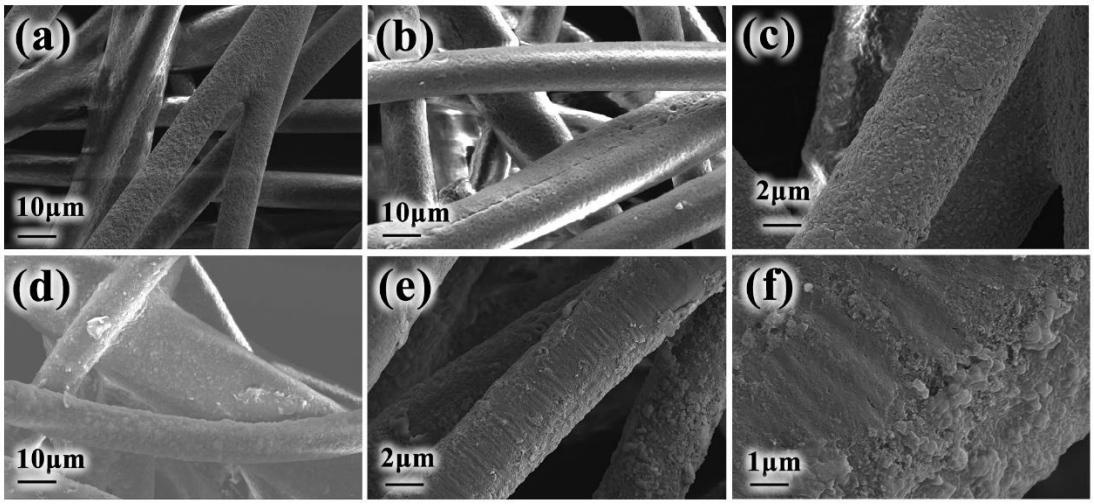

Fig. 3. SEM images of (a) PP/PE SNW, (b) P-GMA, (c)P-HBP, (d) P-HBP-AO, (e) and (f) P-HBP-AO-U.

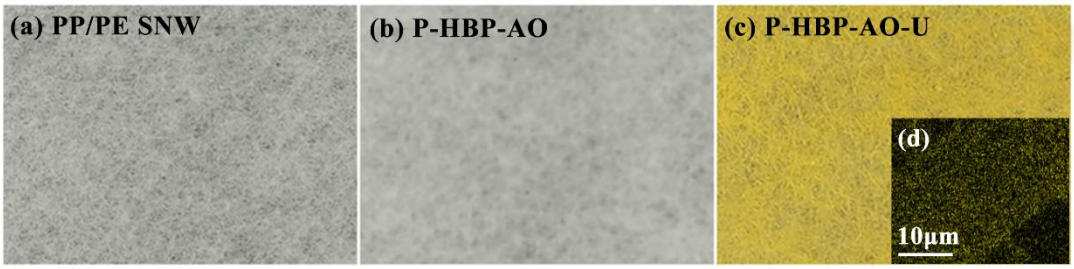

Fig. 4. Images of pristine (a) PP/PE SNW, (b) P-HBP-AO, and (c) P-HBP-AO-U after uranium adsorption. (d) EDS mapping image of uranium.

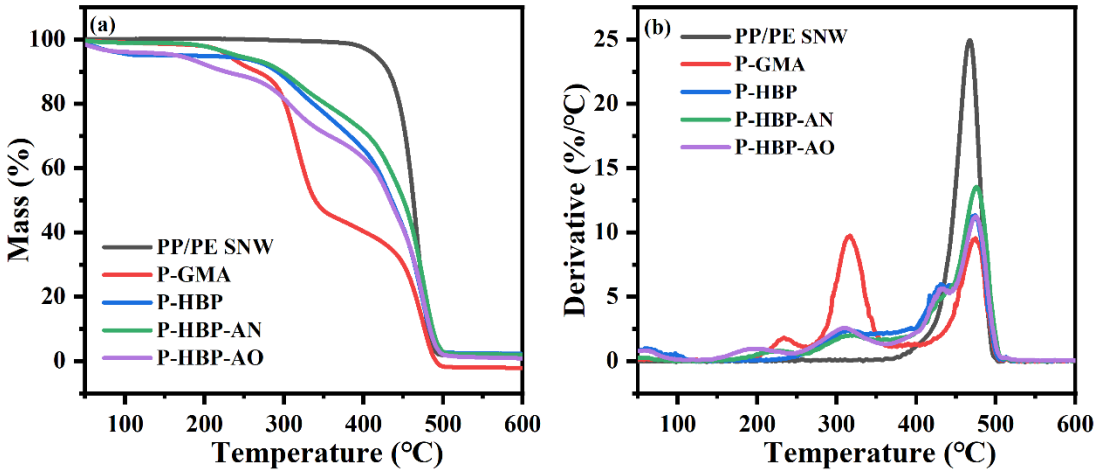

Fig. 5. TG (a) and DTG (b) curves of pristine and modified PP/PE SNW fibers.

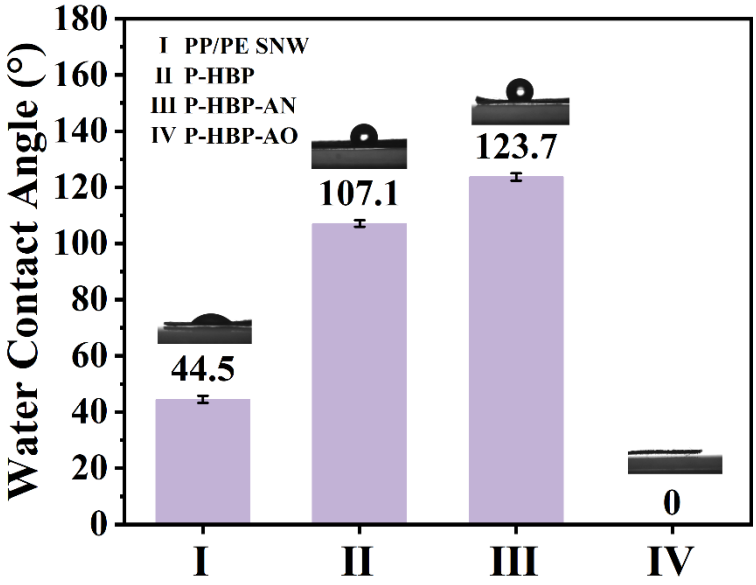

Fig. 6. Water contact angle for PP/PE SNW, P-HBP, P-HBP-AN, and P-HBP-AO

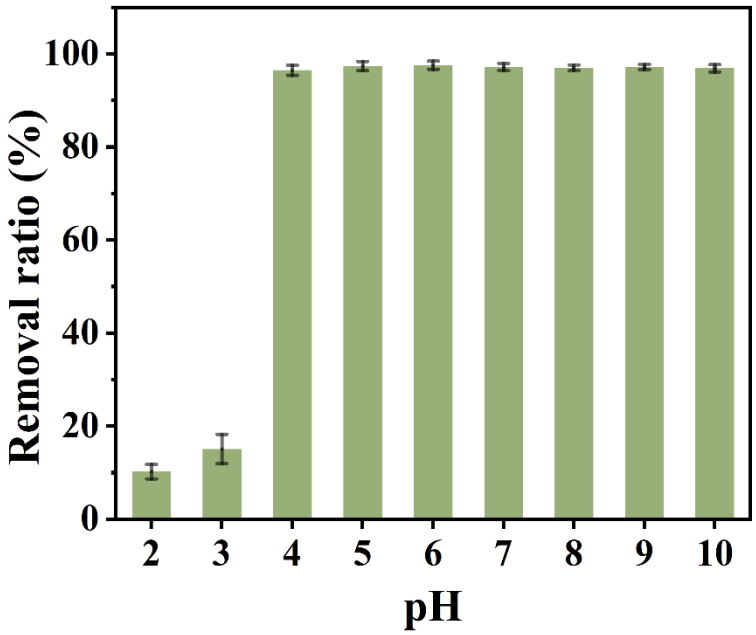

Fig. 7. Effect of pH on uranium removal by P-HBP-AO.

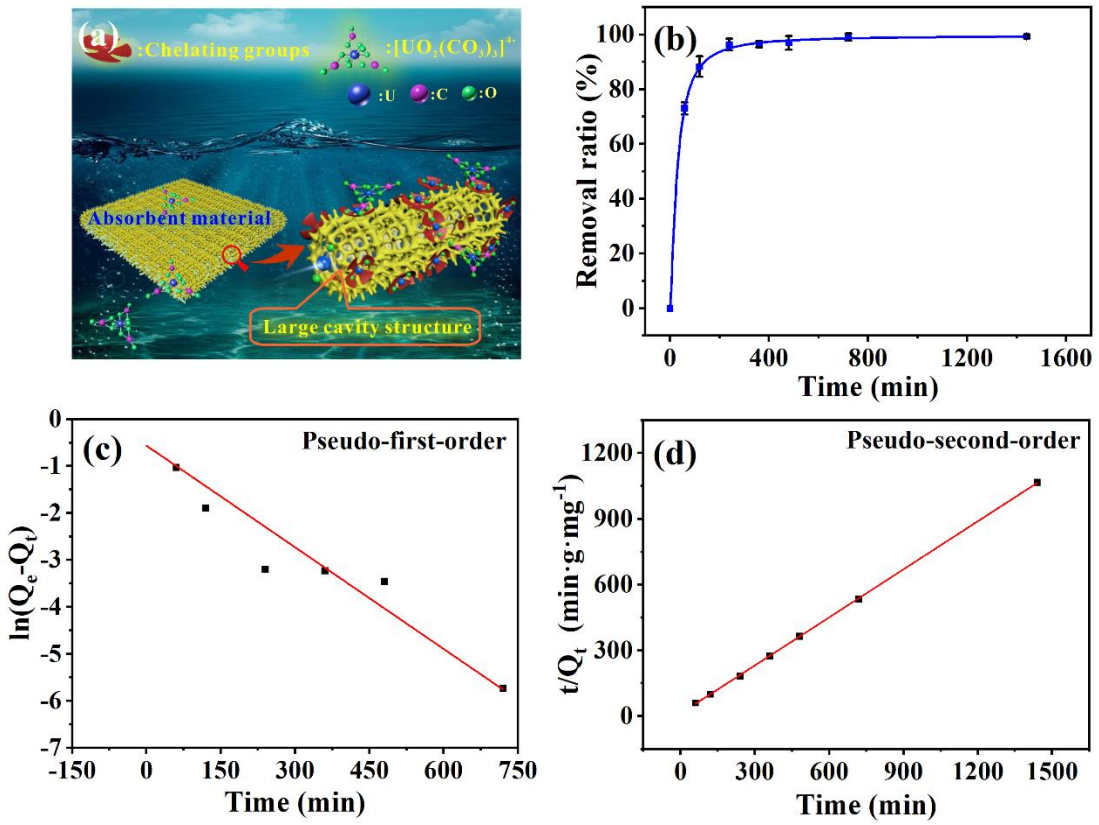

Fig. 8. (a) Branched structure of P-HBP-AO. (b) Removal ratio varied with adsorption time. (c) Pseudo-first-order and (d) pseudo-second-order models for uranium removal by P-HBP-AO

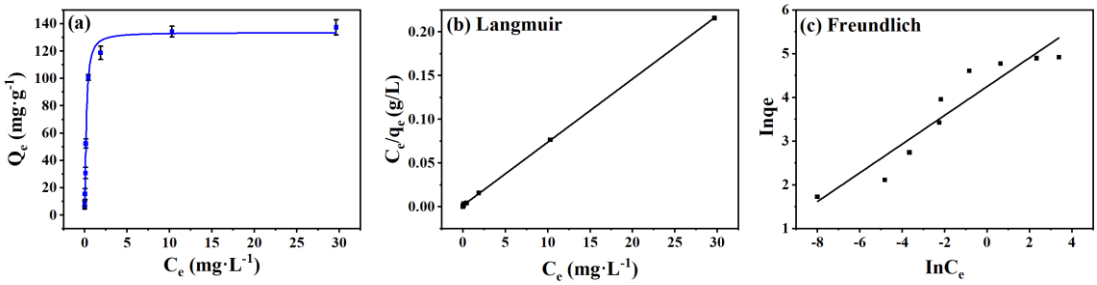

Fig. 9. (a) Adsorption isotherm of P-HBP-AO for uranium. (b) Langmuir and (c) Freundlich isotherms for uranium adsorption by P-HBP-AO.

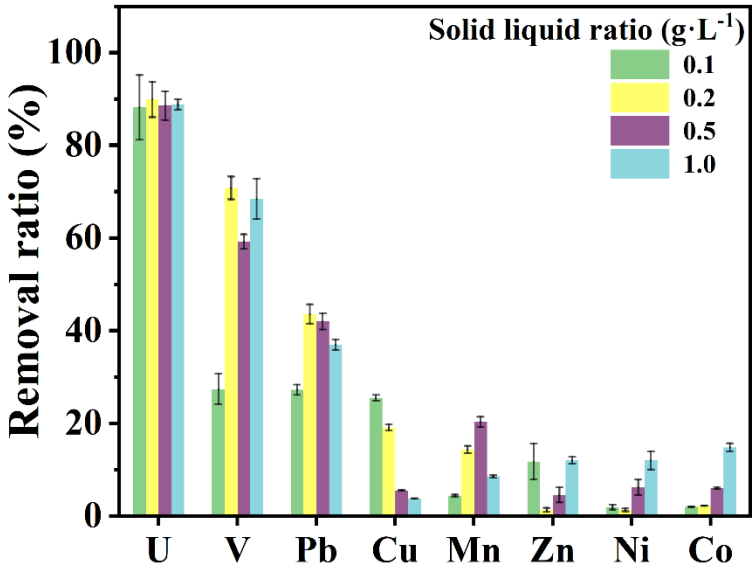

Fig. 10. Adsorption selectivity of P-HBP-AO for uranium.

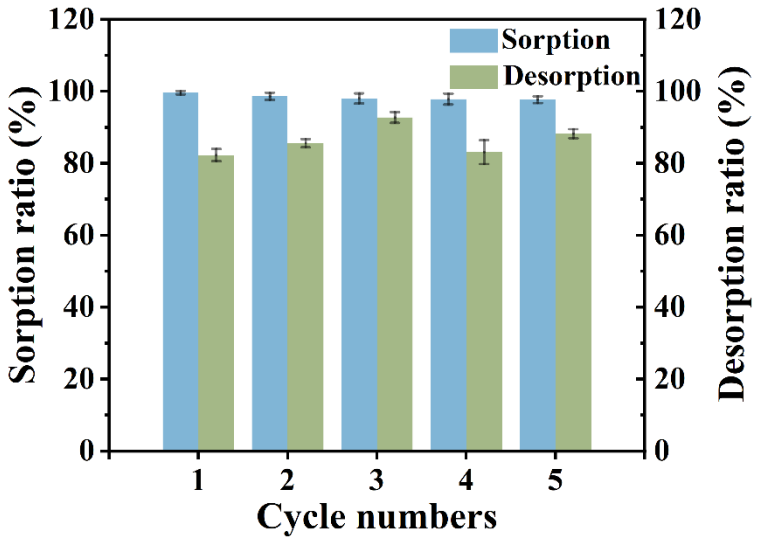

Fig. 11. Desorption and reusability of P-HBP-AO for uranium.

Tables

Table 1. Kinetic parameters for uranium adsorption by P-HBP-AO

Pseudo-first-order adsorption model			Pseudo-second-order adsorption model		
$k_1 \times 10^{-3}$ (min^{-1})	Q_e ($mg \cdot g^{-1}$)	R_1^2	k_2($g \cdot mg^{-1} \cdot min^{-1}$)	Q_e ($mg \cdot g^{-1}$)	R_2^2
7.220	0.570	0.9071	0.045	1.368	0.9999

Table 2. Isotherm adsorption parameters for uranium adsorbed on P-HBP-AO.

Langmuir			Freundlich		
Q_m ($mg \cdot g^{-1}$)	b ($L \cdot mg^{-1}$)	R_L^2	K_F	1/n	R_F^2
138.12	4.993	0.9998	70.10	3.04	0.8937